Eur. J. Mineral.
2005, **17**, 43-55

Garnet zoning in high pressure granulite-facies metapelites, Mozambique belt, SE-Kenya: constraints on the cooling history

CHRISTOPH A. HAUZENBERGER*, JÖRG ROBL and KURT STÜWE

Institut für Erdwissenschaften, Karl-Franzens Universität Graz, Universitätsplatz 2, A-8010 Graz, Austria

Abstract: Three metapelitic samples from the granulite facies Taita Hills, part of the Neoproterozoic Mozambique belt in SE-Kenya, contain nearly pure almandine-pyrope garnets. These garnets show a diffusional zoning of X_{Fe} = Fe/(Fe+Mg) at the rim over a distance of ~200-500 μm if in contact with biotite. Garnet-biotite Fe-Mg exchange thermometry yields closure temperatures between 530-735°C. Diffusion zoning profiles in garnets are used to estimate cooling rates using a numerical model. For the calculations a metamorphic peak temperature and pressure of 820°C and 1.15 GPa are obtained from mafic granulites. Matching of numerically modelled and observed zoning profiles indicates cooling rates between 1-3°C/my. Comparison with cooling rates estimated with the analytical approach of Ehlers & Powell (1994) and with geochronologically derived cooling rates shows that the volumetric ratio of biotite to garnet was about 0.5 during closure. This is consistent with the volumetric ratio observed in thin section, but inconsistent with microprobe analyses that indicate that only biotite in the immediate vicinity of garnet equilibrated with garnet. Conversely, significant garnet zoning only occurs where in contact with biotite. We suggest that these inconsistencies can be explained with changes in the grain boundary processes during cooling: in the thermal evolution above the closure temperature around 735°C a fast grain boundary model applied so that all biotite in the thin section equilibrated with garnet. At lower temperatures local zoning developed, but did not influence the composition of the garnet grain centers. The change in grain boundary process from fast to slow diffusing grain boundaries may correlate with the solidus temperature of the rock.

Key-words: garnet zoning, modelling, slow cooling, granulite facies, Mozambique belt.

Introduction

The origin and evolution of granulite facies rocks in Eastern Africa is related to formation of the Gondwana supercontinent in the Neoproterozoic (Stern, 1994; Shackleton, 1996). Large areas of granulite facies rocks characterized by similar *PT* conditions are exposed at today's surface of Eastern Africa (Appel *et al.*, 1998; Möller *et al.*, 2000; Sommer *et al.*, 2003; Hauzenberger *et al.*, accepted). This observation continues through other adjoining parts of Gondwana including Madagascar, southern India and the East Antarctic Shield (*e.g.*, Stüwe & Sandiford, 1993; Raase & Schenk; 1994; Bhattacharya & Kar, 1998; Jacobs *et al.*, 1998; Markl *et al.*, 2000). Such a puzzling two-dimensionally extensive exposure of rocks of similar age and metamorphic peak conditions raises the question as to the nature of the underlying orogenic process. As a consequence, a number of studies have been concerned with interpreting the orogenic processes responsible for the exhumation of central Gondwana (*e.g.* Stüwe & Sandiford, 1993). One of the key handles on deriving orogenic histories from ancient metamorphic rocks is by constraining their thermal evolution, in particular their cooling rate. Interestingly, slow cooling rates have been documented in a number of terrains of Central Gondwana (Maboko & Nakamura, 1995; Möller *et al.*, 2000; Ganguly *et al.*, 2001; Fernando *et al.*, 2003).

In general, cooling rates of rocks may be determined in three different ways: (1) different closure temperatures of different radiogenic systems may be used (*e.g.* Dodson, 1973; Mezger *et al.*, 1992). (2) The diffusion of stable isotopes between minerals is temperature dependent and their distribution between different minerals can be used to determine the cooling history (*e.g.* Eiler *et al.*, 1992; 1995). (3) Another possibility to reconstruct the thermal history of a rock is by using diffusive chemical zoning in metamorphic minerals (*e.g.* Lasaga, 1983; Florence & Spear, 1995). In this paper we use diffusive zoning profiles in garnet to determine cooling rates of the Neoproterozoic crystalline basement of the Taita Hills in SE Kenya by matching numerically calculated and observed zoning patterns. We follow an approach previously used by a number of authors for example Florence & Spear (1995), O'Brian (1997), Dachs & Proyer (2002), Fernando *et al.* (2003) and others, but refine their modelling by considering a finite grain size explicitly. Our results are compared with analytical calculations of closure temperature using the equations of

*E-mail: christoph.hauzenberger@uni-graz.at

0935-1221/05/0017-0043 $ 5.85
DOI: 10.1127/0935-1221/2005/0017-0043

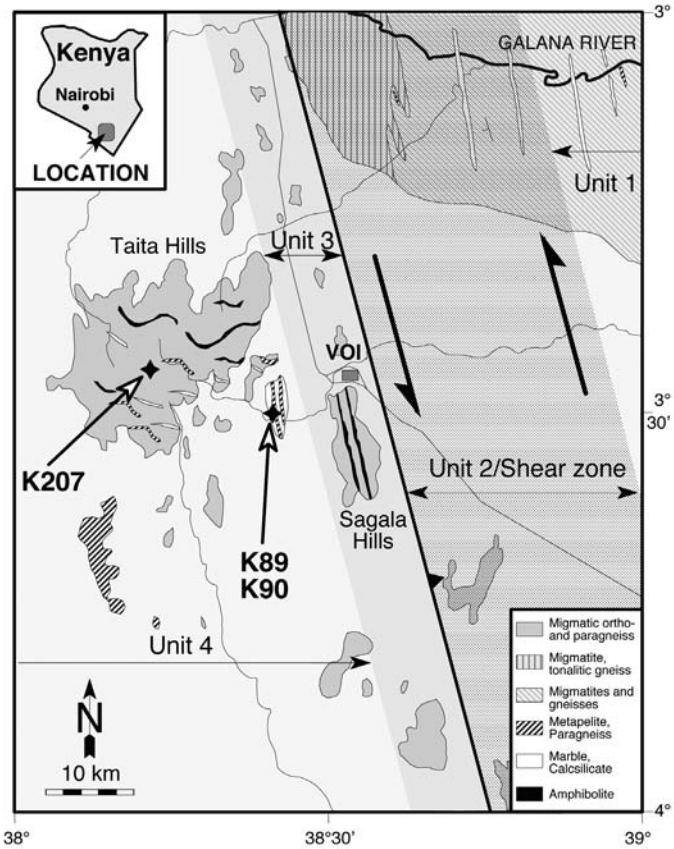

Fig. 1. Simplified geological map of the Taita Hills - Tsavo East National Park area (Galana river).

Dodson (1986) and its modification by Ehlers & Powell (1994) as well as with a geochronologically derived cooling history for the Taita Hills (Hauzenberger, 2003). Finally, we use these results to infer aspects of the exhumation history of the granulites.

Geological setting and sample description

The Taita Hills in SE-Kenya belong to the Mozambique belt (Holmes, 1951) which is part of the Neoproterozoic East African Orogen (Stern, 1994) (Fig. 1). Structurally, the area can be subdivided into 4 units that are described in some detail by Hauzenberger *et al.* (accepted) (Fig. 1). Unit 1 in the eastern most part of the basement along the Galana river is characterised by a subhorizontal foliation. Migmatites and gneisses with intercalated marbles, calcsilicates and metapelites and bands of amphibolites are the dominant rock types. Unit 2 covers the western part of the Galana river and is a *ca*. 25 km wide shear zone with subvertical foliation planes. The eastern part shows similar rocks as observed in unit 1. Towards the west, the dominant rock type changes from metasedimentary units to amphibole-bearing migmatites (metatonalites) with intercalated amphibolites. Unit 3 is a 10 kilometer wide zone (Sagala Hills zone) west of the strike slip zone that defines unit 2. This zone is characterized by elongated and folded felsic migmatic orthogneiss bodies with bands of mafic rocks. Unit 4 is exposed in the Taita Hills and is composed of a slightly north dipping nappe stack. The main rock types are amphibole - biotite - plagioclase - quartz ± garnet ± clinopyroxene ± scapolite bearing migmatic gneisses with mafic intercalations. In the southern part, metapelites, paragneisses, marbles and some amphibolites are common (Parkinson, 1947; Horkel *et al.*, 1979; Pohl & Niedermayr, 1979).

Table 1. Modal analyses of mineral phases in samples K89, K90, and K207 (1000 points counted).

Sample	K89	K90	K207
Grt	36	35	14
Bt	23	18	42
Ky	11	17	2
Sil	14	15	15
Qtz	15	14	15
Pl	0	0	2
Kfs	0	0	10
Rt	1	1	0
Grt*	61	66	25
Bt*	39	34	75

* = normalized to 100

Based on petrological, geothermobarometric and geochronological evidence, two different tectono-metamorphic events are recognised in the region. Units 1 and 2 (Galana river) show similar *PT* conditions of about 760-820°C and 0.75-0.95 GPa, as well as similar age of metamorphism of ~ 560-580 Ma (Hauzenberger, 2003). Units 3 and 4 (Sagala and Taita Hills) show *PT* conditions around 760-840°C and 1.0-1.2 GPa and a slightly older age of metamorphism around ~ 640 Ma (Hauzenberger, 2003; Hauzenberger *et al.*, accepted).

Metapelitic gneisses with garnet - biotite bearing assemblages are only exposed as small intercalations in unit 4 in the Taita Hills and this region forms therefore the focus of this study. Three metapelitic samples were selected (Fig. 1). Sample K89 and sample K90 are garnet - biotite - kyanite - sillimanite - quartz - rutile bearing metapelites (GPS coordinates: S 03°26.802' and E 38°29.043'). They were found in the southeast of the Taita Hills (Fig. 1). Plagioclase and K-feldspar are missing in these samples. The most common mineral is garnet, followed by sillimanite + kyanite, biotite and quartz (Table 1). The unusually high content of Al-rich minerals and the absence of K-feldspar indicate that these samples may be restites and the absence of Ca-bearing phases indicates that they can be described in a relatively simple chemical system. Sample K207 was collected in the central part of the Taita Hills (Fig. 1, GPS coordinates: S 03°23.306' and E 38°22.155'). In contrast to samples K89 and K90, this sample contains abundant K-feldspar as well as some plagioclase. Biotite is the most common mineral phase, followed by sillimanite + kyanite, quartz, garnet, K-feldspar and plagioclase (Table 1).

Analytical technique

Mineral analyses were performed on carbon-coated thin sections at the University of Graz, Austria, using a JEOL

Table 2. Microprobe analyses of garnet, biotite, and feldspars

Sample	k89gt2c	k89gt4r	k90gt1	k90gt2	k207gc1	k207gr2	k89bt1i	k89bt3	k89btm	k90bt5	k90bt3	k207bt4	k207kf5	k207p6c
	garnet						biotite						feldspar	
	core	rim	core	rim	core	rim	incl.*	rim+	matrix	incl.*	rim"	rim#	Kfs	Pl
SiO_2	38.53	38.15	39.34	38.84	37.56	37.72	37.56	37.78	37.35	37.89	38.13	35.91	63.43	64.10
TiO_2	0.03	0.00	0.06	0.00	0.02	0.01	4.49	3.03	3.59	4.87	3.19	3.43	0.00	0.00
Al_2O_3	22.29	21.93	21.35	21.31	21.28	21.19	18.50	18.64	18.04	17.77	17.74	19.04	18.52	22.88
FeO	30.08	31.72	30.56	32.44	32.68	35.14	8.90	11.84	13.39	10.36	12.81	16.56	0.00	0.00
MnO	0.44	0.54	0.53	0.51	1.33	1.77	0.04	0.00	0.00	0.06	0.00	0.00	0.00	0.00
MgO	8.60	7.48	7.72	6.42	6.00	3.95	16.60	15.85	14.47	14.20	13.82	10.32	0.01	0.00
CaO	0.79	0.81	0.91	1.18	0.97	1.33	0.00	0.00	0.00	0.00	0.00	0.00	0.00	3.79
K_2O	0.01	0.01	0.01	0.02	0.03	0.00	9.46	9.53	9.22	9.58	9.35	9.64	14.87	0.21
Na_2O	0.00	0.01	0.01	0.04	0.01	0.03	0.56	0.31	0.24	0.46	0.26	0.14	1.40	9.99
Total	100.77	100.65	100.49	100.76	99.88	101.14	96.11	96.98	96.30	95.19	95.30	95.04	98.23	100.97
Si	2.963	2.962	3.046	3.031	2.971	2.989	2.694	2.717	2.723	2.761	2.797	2.703	2.970	2.809
Ti	0.002	0.000	0.003	0.000	0.001	0.001	0.242	0.164	0.197	0.267	0.176	0.194	0.000	0.000
Al	2.020	2.007	1.948	1.959	1.984	1.979	1.564	1.580	1.550	1.526	1.534	1.689	1.022	1.182
Fe^{3+}	0.052	0.071	0.000	0.000	0.078	0.047	0.000	0.000	0.000	0.000	0.000	0.000	0.000	0.000
Fe^{2+}	1.882	1.989	1.978	2.117	2.084	2.282	0.534	0.712	0.816	0.631	0.786	1.042	0.000	0.000
Mn	0.029	0.036	0.034	0.034	0.089	0.119	0.002	0.000	0.000	0.003	0.000	0.000	0.000	0.000
Mg	0.986	0.866	0.891	0.746	0.707	0.467	1.775	1.699	1.573	1.543	1.511	1.158	0.001	0.000
Ca	0.065	0.067	0.075	0.099	0.082	0.113	0.000	0.000	0.000	0.000	0.000	0.000	0.000	0.178
K	0.001	0.001	0.001	0.002	0.003	0.000	0.866	0.874	0.858	0.891	0.875	0.926	0.888	0.012
Na	0.000	0.001	0.001	0.006	0.002	0.005	0.078	0.043	0.034	0.064	0.038	0.020	0.127	0.849
Sum	8.000	8.000	7.977	7.994	8.001	8.002	7.755	7.789	7.751	7.686	7.717	7.732	5.008	5.030
X_{Fe}	0.656	0.697	0.689	0.739	0.747	0.830	0.231	0.295	0.342	0.290	0.342	0.474		
X_{alm}	0.635	0.672	0.664	0.707	0.704	0.766						X_{kfs}	0.875	0.012
X_{prp}	0.333	0.293	0.299	0.249	0.239	0.157						X_{ab}	0.125	0.817
X_{grs}	0.022	0.023	0.025	0.033	0.028	0.038						X_{an}	0.000	0.171
X_{sps}	0.010	0.012	0.011	0.011	0.030	0.040								

* incl. = biotite inclusion in garnet; + = biotite grain touches garnet, measured spot ~ 10 µm from contact
" = biotite grain touches garnet, measured spot ~100 µm from garnet-biotite contact; # = biotite grain touches garnet, measured spot ~ 400 µm from contact

6310 microprobe equipped with a LINK ISIS energy dispersive system and a MICROSPEC wavelength dispersive system with operating conditions of 15 kV accelerating voltage, 5 nA beam current and ~ 1 µm beam diameter. Elements were calibrated against natural standards. Online ZAF corrections were performed. Garnets in textural equilibrium with biotite were analysed for both rim and core compositions. Some representative garnets, adjacent to biotite were investigated for zoning patterns by running microprobe line profiles across the grains, at a 2-5 µm spacing. Mineral abbreviations after Kretz (1983) are used.

Mineral chemistry, petrography and garnet zoning

Samples K89 and K90 are nearly identical with respect to mineral assemblage, modal abundance and chemical composition of minerals (Tables 1, 2). Sample K207 contains more biotite and also bears plagioclase and K-feldspar. However, all three samples are similar enough in mineral assemblage and composition so that they are discussed together.

Garnets from all samples are almost pure almandine - pyrope solid solutions with a general range of X_{Alm} = Fe/(Fe+Mg+Ca+Mn) around X_{Alm} = 0.64 to X_{Alm} = 0.83. Apparent grain size in thin section varies from about 0.3 to 7 mm in diameter. Mineral inclusions of quartz, rutile, sillimanite, and biotite as well as small fractures are commonly observed. Garnet grains adjacent to biotite show distinct retrograde diffusive zoning, while such a zoning is not observed in garnet bordered by quartz, kyanite, or sillimanite. To document this pattern in detail, several line profiles across garnet in contact with different mineral phases, as well as a two dimensional profile across a garnet rim in contact with biotite and quartz, were performed. Figure 2 shows back scattered electron images of several garnet grains from the three samples. The dark lines indicate the position where zoning profiles were analysed (Fig. 3).

In Fig. 2a a garnet grain with a section diameter of ~ 7 mm contains many inclusions as well as some fine fractures. The measured zoning profile A-B across the garnet touches on both rims biotite. Over a distance of ~ 0.5 mm an increase of X_{Alm} towards the rim is observed (Fig. 3a). However, in the vicinity of fine fractures which are partly filled with Fe-oxides or biotite flakes, the X_{Alm} also

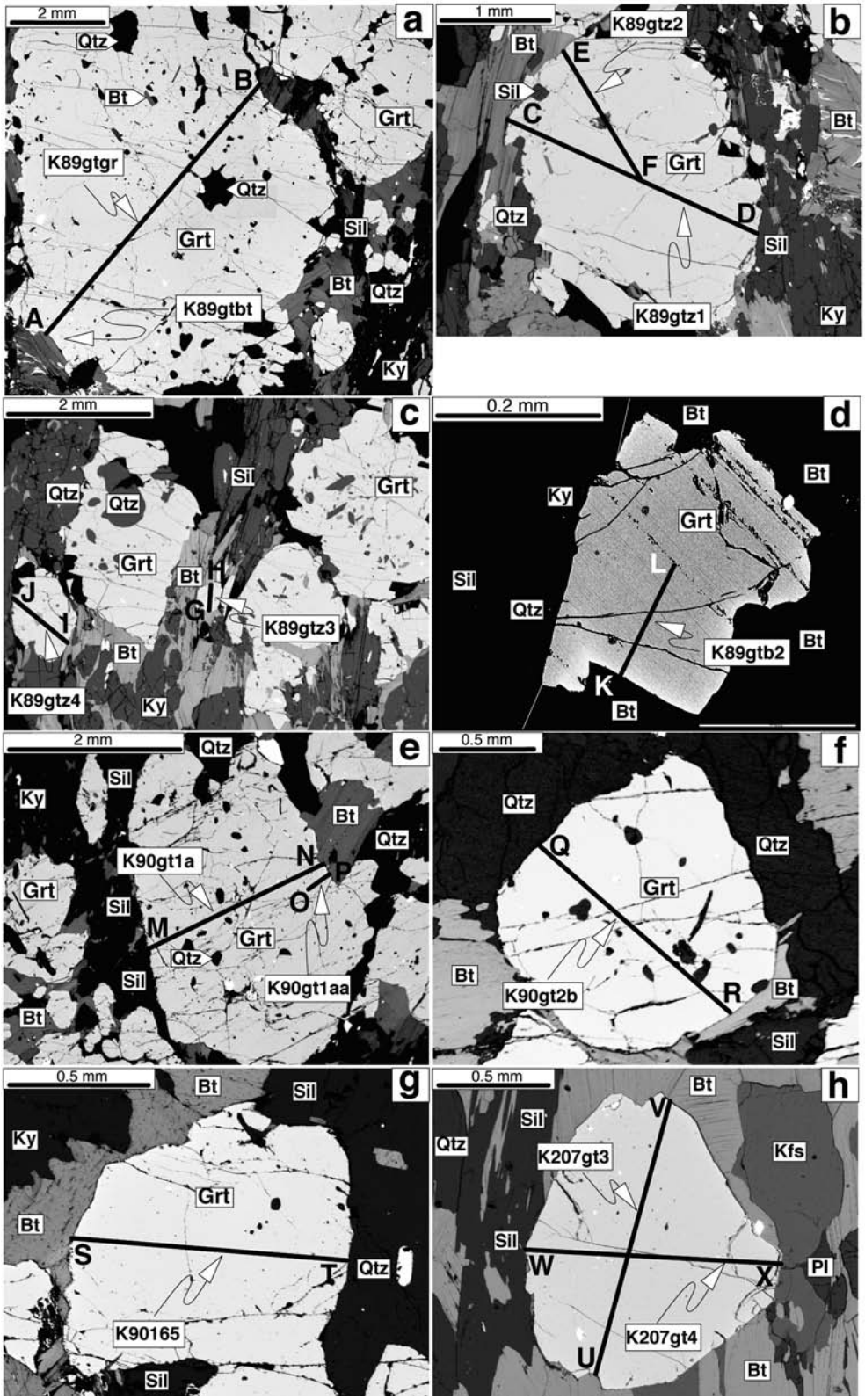

Fig. 2. Backscattered electron images of the garnet - biotite - sillimanite - kyanite - quartz ± K-feldspar ± plagioclase ± rutile bearing samples K89 (a-d), K90 (e-g), and K207 (h). The black lines indicate the location of the analysed chemical composition profiles.

increases. In Fig. 2b a ~ 2.5 mm large garnet section partly touching biotite, partly touching quartz and sillimanite is shown. The chemical zoning profile across C-D (Fig. 3b) shows a decrease in X_{Alm} towards biotite over a distance of ~ 0.2-0.3 mm. At the opposite garnet rim which is touching sillimanite, no change in X_{Alm} is observed. The chemical zoning profile E-F, which runs from the garnet rim in contact with biotite to the garnet core (Fig. 2b) shows exactly the same shape and decrease in X_{Alm} (Fig. 3c). An inclusion of quartz and altered biotite slightly increases the

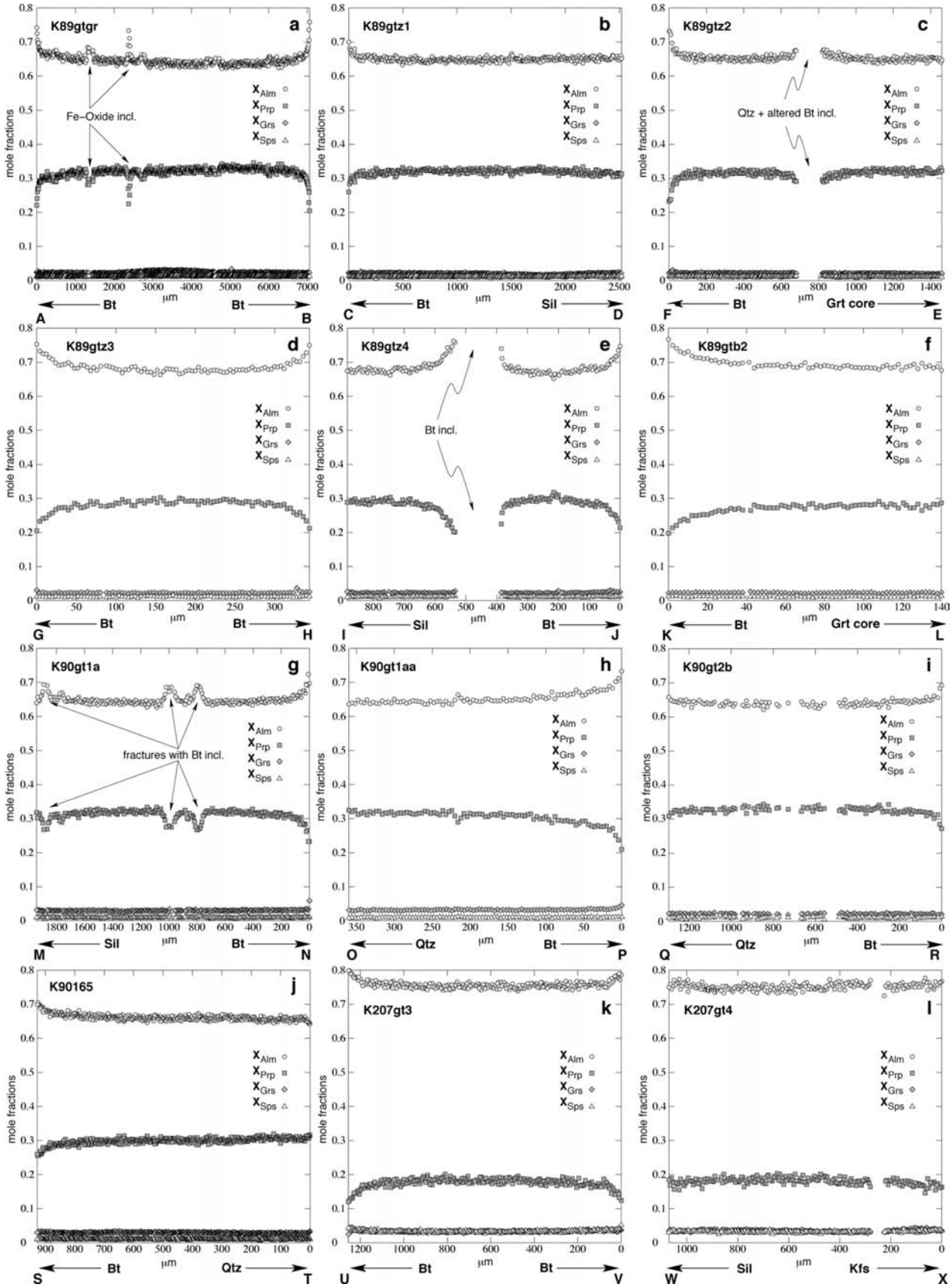

Fig. 3. Garnet zoning pattern of almandine, pyrope, grossular and spessartine along lines depicted in Fig. 2. Profiles were assembled from closely spaced quantitative spot analyses of garnet. Note that X_{Prp} decreases and X_{Alm} increase at the biotite contacts whereas no X_{Grs} and X_{Sps} change is observed. No significant variation is observed when garnet is in contact with either quartz, sillimanite, kyanite, or feldspar.

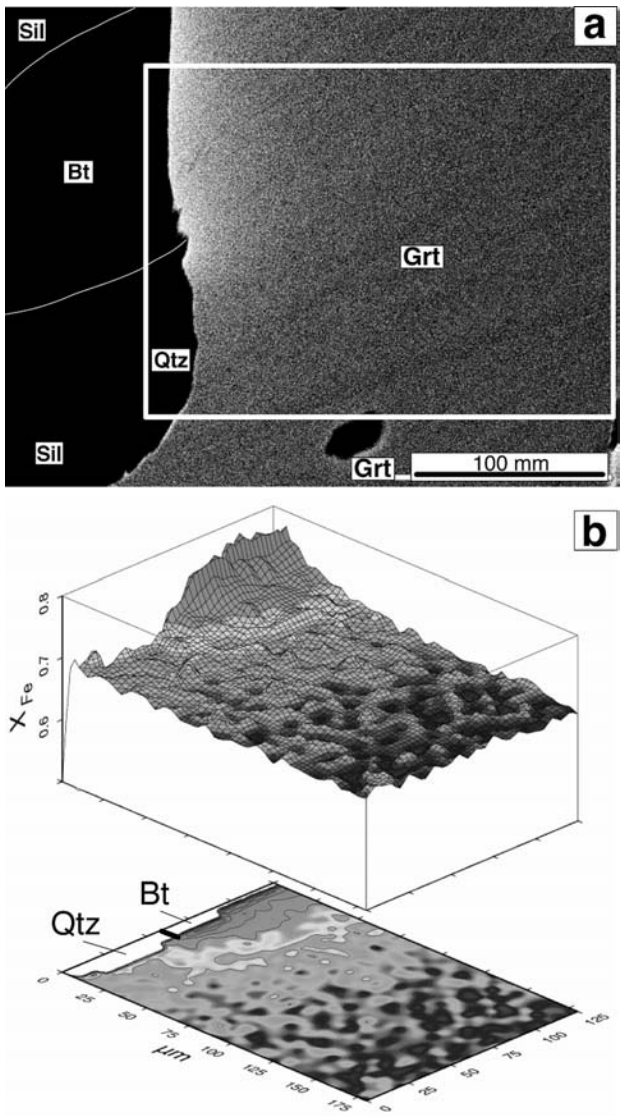

Fig. 4. Compositional map of X_{Fe} of garnet in contact with biotite, sillimanite and quartz in sample K89. (a) is a backscattered electron image of the contact. (b) 3 dimensional image of a 2 dimensional spot analyses of (a). The X_{Fe} zonation along the grain boudary and within garnet is very similar. The spatial resolution of the analysis plot in Fig. 4b is 5 µm.

X_{Alm}. This pattern is particularly nicely illustrated in Fig. 4 where the analysis of a detail of a triple junction between garnet, biotite and quartz is shown. An increase of X_{Fe} = Fe/(Fe+Mg) from garnet core to rim is only observed if biotite is in contact with garnet. Quartz in contact with garnet does not influence the X_{Fe} of garnet. In Fig. 2c two smaller garnet sections are shown (~ 0.36 and 0.87 mm). The smaller garnet section is completely surrounded by biotite. The zoning profile (G-H; Fig. 3d) shows on both rims an increase in X_{Alm}. The X_{Alm} analysed at the apparent garnet core is slightly higher than that found in larger garnet section. The pattern of some hundreds of µm of zoning near biotite and the absence of zoning at other garnet contacts is repeated in garnets of other sizes and inclusion density from sample K89 as shown in Fig. 2c,d and Fig. 3e,f.

The chemical composition and zoning profiles of garnets from sample K90 are very similar to garnets from sample K89 (X_{Alm} = 0.64-0.72). Figure 2e shows a ~ 2 mm sized garnet section with several inclusions and fine fractures. Again, towards biotite a ~ 0.3 mm wide rim with increasing X_{Alm} is developed (Fig. 3g). A detailed zoning profile of the garnet rim along the line O-P (Fig. 2e) is shown in Fig. 3h. Figures 2f,g show 2 smaller garnet sections (~ 1 mm) with X_{Alm} increasing towards garnet rim in contact with biotite (Fig. 3i,j). In Fig. 2h a 1.3 mm sized garnet grain section of sample K207 is seen. This sample differs by its mineral assemblage from samples K89 and K90. The chemical composition of garnet is slightly almandine richer: X_{Alm} = 0.75-0.83. The observed garnet zoning is very similar as seen in samples K89 and K90. Retrograde diffusional zoning in garnet is only observed at the contact with biotite. All other minerals phases do not effect the chemical composition of garnet rims. This is shown by the line profiles U-V and W-X (Fig. 3k,l).

Biotite grains do not show any chemical zoning but their X_{Fe} differs slightly by their textural position. Biotite inclusions in garnet usually have the lowest X_{Fe} in samples K89 and K90. Biotite grains in contact with garnet have a slightly higher X_{Fe}. Matrix biotites (no grain boundary with garnet) have the highest X_{Fe} values (Table 2). This could not be observed in sample K207. The chemical composition of both feldspars in sample K207 is homogeneous with X_{Ksp} = 0.88 for K-feldspar and X_{Ab} = 0.82 for plagioclase. The aluminosilicate phases kyanite and sillimanite are found in all samples. Some kyanite grains show small sillimanite needles at the rim.

Metamorphic conditions

The zoning profiles described above indicate that garnet-biotite equilibria formed by diffusion and are not useful to extract the peak metamorphic conditions. Therefore, mafic granulites from the vicinity of the localities of samples K89, K90, and K207 were used to determine the peak metamorphic conditions. These rocks have the mineral assemblage garnet - clinopyroxene - hornblende - biotite - plagioclase - quartz ± scapolite. TWEEQU (Berman & Brown, 1992) calculations using garnet - clinopyroxene - biotite - plagioclase - quartz equilibria constrain the peak of metamorphism at 810-830°C at 1.1-1.2 GPa (Fig. 5a). Following the peak of metamorphism, occasional new growth of fibrolite and muscovite in metapelitic rocks and actinolite in mafic rocks indicates an overprint at amphibolite facies conditions during cooling. Garnet core compositions calculated with matrix biotite yield the highest temperatures around ~ 730°C, which is significantly lower than estimated peak *PT* from mafic granulites. Garnet rims and biotites in contact with garnet as well as biotite inclusions in garnet give even lower temperatures of around 530-600°C. In summary, garnet - biotite thermometry indicates throughout temperatures significantly below the metamorphic peak (Fig. 5b). This confirms that the zoning profiles described above formed entirely during retrograde re-equilibration during cooling

from the last metamorphic cycle and can therefore be used for diffusion modelling of the cooling rate of this event only.

Determination of cooling rates from garnet profiles

The distribution of cations in garnet in equilibrium with biotite is temperature dependent and zoning profiles in garnet can therefore be used to infer aspects of the thermal evolution (Florence & Spear, 1995; Ganguly *et al.*, 2000). Dodson (1973) showed that cooling rates may be directly inferred from the closure temperature of garnet centres and expanded this approach in 1986 to an analytical description of entire closure profiles. This approach was expanded to finite grain size of both exchanging grains by Ehlers & Powell, (1994) and Powell & White (1995). Here we used the approach of matching numerically modelled zoning profiles with those measured in thin section (described in Fig. 2 and 3). A numerical model is neccessary, because the investigated rocks contain biotite garnet volume ratios (z) between 0.5 and 3, while the analytical description of Dodson (1986) applies only for infinite biotite reservoir. An "infinite reservoir" can be assumed if the biotite-garnet ratio z is in excess of 5. Conversely, the modification of Ehlers & Powell (1994) for finite volumetric ratios was only done for a plane sheet model neglecting the spherical geometry of most garnet biotite equilibria.

A total of five zoning profiles were selected from the grains discussed in Fig. 2 and 3 for modelling. Note that one of the major differences between samples K89, K90 and sample K207 is that the former two are characterised by a volumetric biotite : garnet ratio z = ~ 1 : 2, whereas this ratio z = ~ 3 : 1 in sample K207. A range of apparent grain sizes and zoning profiles in thin-sections were analysed. Zoning profile A-B (Fig. 2a, 3a) is from the crystal with the largest apparent grain size in thin section (apparent radius = r' = 3.5 mm in sample K89). Zoning profile C-D (Fig. 2b, 3b) is from a somewhat smaller crystal section (r' = 1.2 mm) from the same sample. The next smaller apparent grain size is zoning profile M-N (Fig. 2e, 3g) from sample K90 with r' = 0.97 mm. Finally, we selected the smallest apparent grain size of profile G-H for further investigation (Fig. 2c, 3d with r' = 0.17 mm). Of sample K207, only one zoning profile from a grain with an apparent radius r' = 0.63 mm was selected (profile U-V on Fig. 2h, 3k). In order to compare the analysed zoning profiles with those numerically modelled in a binary system, the zoning profiles were recalculated to X_{Fe} = Fe/(Fe+Mg) and are shown on Fig. 6.

The grain radii reported above are apparent grain size in thin section and care must be taken with interpreting their shape. However, the grains of profiles A-B and C-D were cut through their centres so that this apparent grain size corresponds to the real grain size. The grain of profile A-B was exposed on three sides of the thin section block and the grain of profile C-D on two, so that it was easy to ensure a central cut. Of the other three grains the section position is unknown. We use therefore initially only those two grains for our analysis.

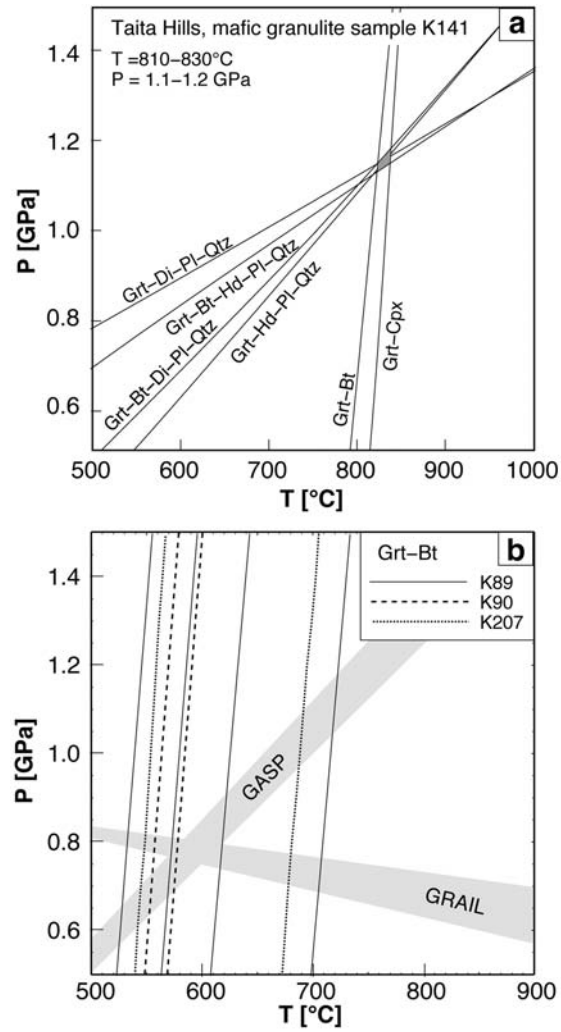

Fig. 5. (a) The *PT*-diagram was calculated with TWEEQU (Berman & Brown, 1992) and mineral core compositions of garnet, clinopyroxene, biotite, and plagioclase from the mafic granulite sample K141, Taita Hills. (b) The garnet - biotite thermometer using garnet core and rim compositions together with biotite in contact with garnet and matrix biotite results in significantly lower temperatures. The pressure was calculated with the GASP (garnet-aluminosilicate-quartz-plagioclase) and GRAIL (garnet-rutile-ilmenite-aluminosilicate-quartz) barometers.

Model and boundary conditions

In our modelling we have followed the approach used by many authors in which the diffusion equation in spherical coordinates is coupled with a thermometer equation and a *Kd* expression to formulate the boundary conditions (Lasaga, 1983; Florence & Spear, 1995). The Arhenius relationship is used to describe the temperature dependence of diffusivity. This approach is summarised in the appendix but some parameters require discussion here.

Diffusion coefficients

Experimentally derived values for diffusion of Fe and Mg in garnet vary by several orders of magnitude (*e.g.*,

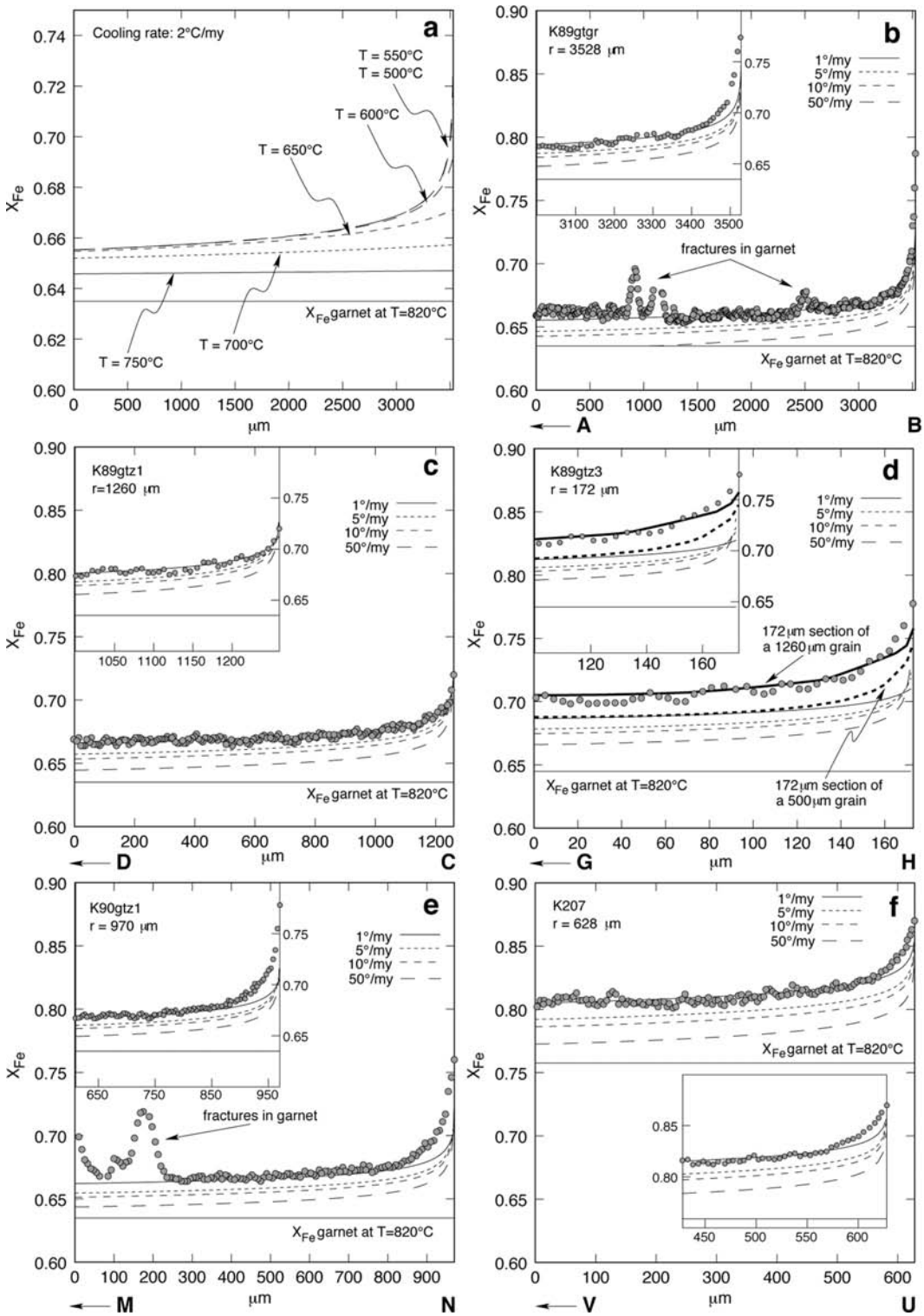

Fig. 6. (a) Time dependent evolution of a calculated zoning profile. (b-f) Comparisons of calculated X_{Fe} = Fe/Fe+Mg closure profiles for four different cooling rates with measured X_{Fe} of profiles from Fig. 2 and 3. Note, that for most measured profiles the best fit is for a closure profile with s = 1°C/my, except in (d) which is related to a sectioning effect. The thick line in (d) is discussed in the text.

Cygan & Lasaga, 1985; Ganguly *et al.*, 1998). The most recent Fe-Mg diffusion coefficients determined by Ganguly *et al.* (1998) were used here. It is also assumed that the diffusion of Fe-Mg in biotite is several orders of magnitude faster than in garnet so that internal chemical zoning in biotite can be neglected during modelling (Dodson, 1973).

Initial conditions

Geothermometry has shown that temperatures of all garnet grains are lower than the peak metamorphic conditions so that the garnets were completely reset during cooling. This is also confirmed by the smooth shape of the zoning profiles indicating diffusion as the

Table 3. Garnet parameters for the model calculations.

Line #		K89gtgr	K89gtz1	K89gtz3	K90gtz1	K207
1	Volumetric ratio Bt/Grt	0.500	0.500	0.500	0.500	3.000
2	Apparent radius r' [mm]	3.528	1.260	0.172	0.970	0.628
3	X_{Fe}^{Grt}	0.656	0.657	0.700	0.689	0.800
4	X_{Fe}^{Bt} matrix (Btm)	0.342	0.342	0.342	0.342	0.474
5	X_{Fe}^{Bt} in contact to Grt (Bt')	0.295	0.295	0.295	0.295	0.474
6	X_{Fe}^{Grt} re-calculated at T = 820°C	0.632	0.632	0.632	0.662	0.757
7	X_{Fe}^{Bt} re-calculated at T = 820°C	0.353	0.353	0.353	0.383	0.497
8	*Tc* [°C] (Grt - Btm)	737	735	648	669	652
9	*Tc* [°C] (Grt - Bt')	642	640	568	585	652
10	*s* [°C/my] (Dodson eq.) Btm	0.040	0.330	0.700	0.050	0.060
11	*s* [°C/my] (Ehlers & Powell, 1994) Btm	0.300	2.200	4.800	0.330	0.090
12	*s* [°C/my] (Dodson eq.) Bt'	0.001	0.010	0.020	0.002	0.060
13	*s* [°C/my] (Ehlers & Powell, 1994) Bt'	0.010	0.070	0.150	0.010	0.040

Btm = matrix biotite; Bt' = biotite in contact with garnet; Tc = closure temperature

The X_{Fe}^{Grt} in the 3rd line is that of the apparent grain center as seen on Fig. 6. The X_{Fe}^{Bt} is from Table 2. The recalculated X_{Fe}^{Bt} and X_{Fe}^{Grt} are those at the metamorphic temperature peak using the *Kd* expression (eq. 5) and the mass balance equations 8-11. The closure temperatures listed in the 8th and 9th line are those calculated from garnet core composition (3rd line) with matrix biotite and biotite near garnet in the 4th and 5th line, respectively. The theoretical equilibrium composition of garnet and biotite was recalculated at 735°C using eq. 5 and eqs. 8-11 and was found to be similar to the analysed ones (line 8). The cooling rates listed in the last 4 lines are those calculated with Dodson (1986) (eq. 7 in Appendix) and its extension for finite grain sizes by Ehlers & Powell (1994) (eq. 12).

principal control on zoning. As a consequence, the closure profile is independent of older compositional variations (Dodson, 1973) and we can assume that both garnet and biotite were of homogeneous composition at the metamorphic peak around 820°C. However, this assumption is not sufficient: Dodson (1973) has shown that the ratio of biotite to garnet must be infinite so that changes in composition of biotite during cooling can be neglected. Thus, the modal ratio of biotite to garnet between 1:2 and 3:1 requires that the starting composition of both phases are known and the composition of biotite during cooling is tracked via mass balance considerations.

The initial compositons were calculated using the modal abundances of garnet and biotite (Table 1) to calculate the bulk Fe-Mg content of the rock. The equilibrium *Kd* between garnet and biotite was then calculated using this bulk composition at 820°C. This was done by simultaneously solving the mass balance- and equilibrium coefficient equations for Fe and Mg exchange (see appendix). For these calculations it was assumed that no mineral growth or resorbtion (net transfer reaction) occurred during cooling. This assumption is supported by the fact that no retrograde growth of any high temperature phases can be observed. Results are presented in Table 3. Using these parameters and initial conditions, time dependent zoning profiles during cooling were calculated until they are frozen and changes are small. Figure 6a shows that the zoning process is effectively terminated below about 600°C. Final zoning profiles (termed "closure profiles") were obtained for a range of cooling rates, namely 1, 5, 10 and 50°C/my.

Results

The calculated closure profiles plotted in Fig. 6b-f all have similar characteristics regardless of grain size: at high cooling rates, mass transfer by diffusion is only accomplished over a short period of time and garnet compositions change only slightly. The slope of the X_{Fe} curve at the garnet rim is steep (Fig. 6b-f). Slower cooling rates enhance Fe-Mg exchange between garnet and biotite. Hence, X_{Fe} of garnet shows its highest values and the slope of the X_{Fe} curve at the rim is less steep.

The zoning profiles of the two grains that are known to cut through the centers are best matched by a numerically modelled closure profile assuming a cooling rate of 1°C/my (Fig. 6b,c). A-B has a very good match, nevertheless, close to the rim some discrepancies are observed. The analysed profile increases its X_{Fe} slightly further inwards as calculated (see inset of Fig. 6b). The garnet zoning profile C-D is perfectly reproduced by the calculated profile for a cooling rate of 1°C/my (Fig. 6c).

The zoning profile along the line G-H of the smallest apparent grain size ($r' = 0.17$ mm) of sample K89 (Fig. 2c) is not matched by any of the calculated zoning profiles. The small radius of the grain section, the higher X_{Fe} in the core and the rim, and the different shape of the zoning at the rim are evidence, that the analysed profile belongs to a garnet grain cut somewhere at the edge. The zoning profile along the line M-N ($r' = 0.97$, Fig. 6e) is best fitted with the closure profile for a cooling rate of 1°C/my. The increase in X_{Fe} at the rim differes slightly. The garnet zoning profile from sample K207 (profile U-V; $r' = 0.63$ mm) is well reproduced by calculated

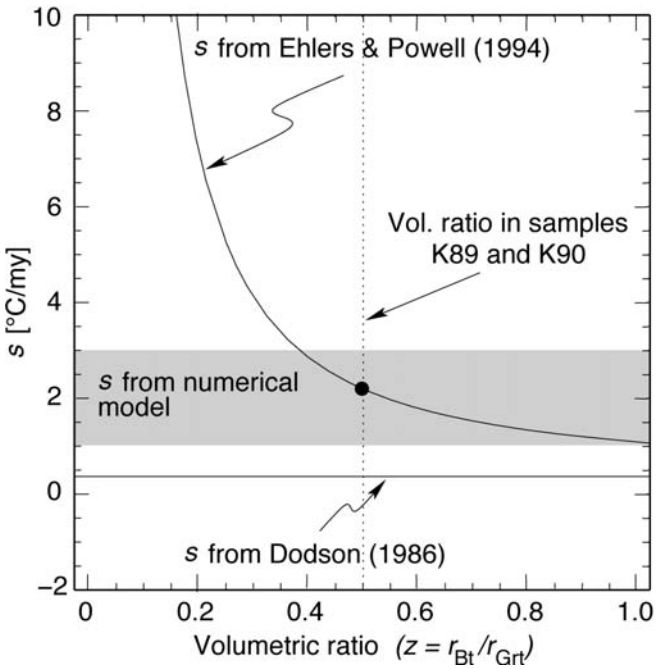

Fig. 7. The effect of changes in volumetric ratio between biotite and garnet (horizontal axis) on estimated cooling rate (vertical axis). The curve in the diagram was calculated with eq. 12. Note that a volumetric ratio of biotite to garnet of $z = 0.5$ gives consistent cooling rate estimates, while a smaller ratio would give much too large estimates.

closure profiles between 1°C/my and 5°C/my (Fig. 6f), which is slightly faster than found in other samples.

Discussion

The results presented above show a good agreement between modelled and measured zoning profiles. They all indicate slow cooling rates between 1 and 3°C/my. In fact, the two grains known to be cut through their centers show an almost perfect match between measured and calculated zoning profiles. Minor differences near the margin of profile A-B may be due to an irregular grain size or due to slower cooling at lower temperatures.

Interestingly, only the grains with an unknown section position show a bad match between measured and calculated zoning profile, which is attributed to the fact that the calculated profiles are for central cuts, while the measured profiles are for sections through the grain margin. In order to investigate this hypothesis, the closure profile of grain section G-H ($r' = 0.172$ mm; Fig. 6d) was modelled assuming that it represents a marginal cut through a grain that is 1.26 mm in radius (as modelled in Fig. 6c). The section position through this much larger grain was adjusted so that its apparent diameter is $r' = 0.172$ mm. This is shown on Fig. 6d as the thick line which may be directly derived from Fig. 6c by geometrical arguments. It may be seen that there is a good match between modelled and measured closure profiles for all considered garnet grains if the sectioning effect is considered. We therefore conclude that a cooling rate of ~ 1-3°C/my is confirmed by the zoning profiles of all investigated garnet grains, pending on the correct choice of diffusion coefficients and other model parameters. The influence of these parameters is now discussed.

Diffusion parameters

All calculations presented above were performed using the diffusion data of Ganguly *et al.* (1998). Clearly, the use of other diffusion data shifts the results accordingly. For example the classic data published by Cygan & Lasaga (1985) results in closure temperatures that are about 100°C lower and in cooling rates that are roughly 20 times as large as those presented here. However, it will be shown below that the cooling rates estimated with the data of Ganguly *et al.* (1998) are nicely consistent with those obtained with geochronological methods so that we suggest that the geochronology provides an independent confirmation of the data published by Ganguly *et al.* (1998).

The grain size effect

The two dimensional zoning shown in Fig. 4 and in the change in biotite composition with proximity to garnet implies a change in the effective volumetric ratio between biotite and garnet during cooling and questions several of the simplifying assumptions made above. Thus, in order to test the effect of changing volumetric ratios we have compared the numerical modelling results with analytical calculations using the equation of Dodson (1986) and its empirical modification by Ehlers & Powell (1994). The results are shown in the last four lines of Table 3 and we discuss these results here only for the grain K89gtz1 where there is the best match between numerically modelled and measured zoning profile. For this grain, Table 3 shows that the cooling rate obtained with Dodson's equation is smaller than the numerically derived cooling rate of 1-3°C/my. This may be ascribed to the fact that Dodson's equation only applies if there is an infinite excess of biotite over garnet. Thus, we also compared our numerical results with the cooling rate estimated with the empirical modification of Ehlers & Powell (1994) for finite grain sizes. It may be seen that the analytical result matches with the numerically calculated result (Fig. 7).

We suggest that the good fit of the two results may be interpreted in terms of the grain boundary processes: as seen in Fig. 3 and 4, diffusion along grain boundaries appears to be very limited. Nevertheless, analytical estimates of cooling rate all give consistent results between 1 and 3°C/my for the cooling rate if a volumetric ratio between biotite and garnet is assumed that considers a fast grain boundary model, *i.e.* that all biotite in the thin section was in equilibrium with the slow diffusing garnet (Fig. 7). Indeed, these estimates are also consistent with geochronologically derived cooling rates (see below). A smaller ratio of biotite : garnet (as implicit in Fig. 4 and in the fact that only a minor proportion of biotite near garnet has a different composition) results in dramatically higher

cooling rate estimates (Fig. 7). We therefore interpret that a fast grain boundary model applied to the garnets considered here in the temperature range between the metamorphic peak and the closure temperature around 735°C. Then the grain boundary diffusion became sluggish and the two dimensional zoning shown on Fig. 3 and 4 developed. The seizure of fast grain boundary diffusion below 735°C may correlate with the solidus temperature of the rocks where wetting of grain boundaries with melt terminated.

Geological relevance and application

We have shown that compositional zoning in garnet from granulite facies rocks of SE-Kenya, Taita Hills can be used to support a slow cooling history. SHRIMP U-Pb zircon dating of orthogneisses in the Taita Hills yielded an age of ~ 640 Ma (Hauzenberger, 2003) which is interpreted as the timing of peak metamorphism. The cooling history of the basement rocks started with a cooling rate of 1-3°C/my at ~ 640 Ma, ~ 820°C and ~ 1.15 GPa. During this early period diffusion in garnet is fast and garnets are homogeneously reset. Further cooling to lower temperatures at about the same cooling rate reduced volume diffusion in garnet producing the observed retrograde rims in garnet. The deduced slow cooling rate indicates a prolonged crustal residence time and slow ascent of this basement unit. A Sm-Nd garnet age of ~ 590 Ma (Hauzenberger, 2003), which is believed to record the time at temperatures around 600-700°C (Mezger *et al*., 1992) in slow cooling areas, and a Ar/Ar hornblende age of ~ 560 Ma (Bauernhofer, 2003), which records the time at temperatures of ~ 500°C (Lee, 1993) indicate cooling rates of 3-5°/Ma (Fig. 8).

Acknowledgement: Financial support by FWF 12375-GEO is gratefully acknowledged. We thank the associate editor and Roger Powell for their critical comments, which helped to improved the manuscript.

Appendix

In our model, chemical zonation evolves while the garnet cools with elapsing time. The time - temperature evolution is described by a linear cooling function:

$$T_t = T_i - ts \quad (1).$$

The temperature (T) decreases from the starting temperature (T_i) with time (t) at the cooling rate s. The temperature dependence of the diffusivity of Fe and Mg was calulated using the Arrhenius relationship:

$$D = D_0 e^{\frac{Q}{RT}} \quad (2).$$

D stands for the diffusivity, R for the gas constant and T for the absolute temperature. D_0 and Q are the pre-exponent diffusivity and the activation energy, respectively. We used the diffusion constants of Ganguly *et al.* (1998): $D_0^{Mg} = 4.66 \times 10^{-9}$ m^{2}s^{-1}, $D_0^{Fe} = 3.50 \times 10^{-9}$ m^{2}s^{-1}, $Q_{Mg} = 274186$ Jmol^{-1}, $Q_{Fe} = 254220$ Jmol^{-1}. The diffusivity for the inter-diffusion of Fe and Mg is assumed to depend on the concentration of Fe and Mg according to:

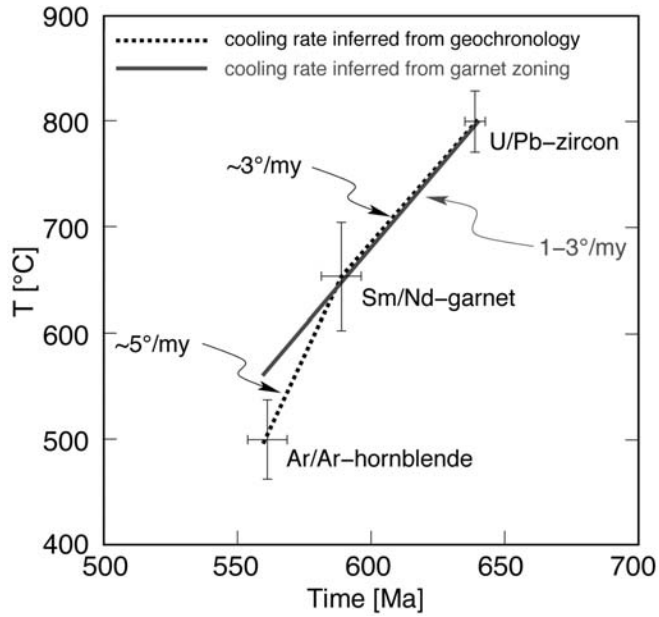

Fig. 8. Calculated cooling paths of granulites from the Taita Hills, SE-Kenya from this study (solid line) compared with cooling rates inferred from geochronology (dotted line; Hauzenberger, 2003). The SHRIMP U-Pb zircon ages of ~ 640 represent the age of peak metamorphism in this area.

$$D_{Fe\text{-}Mg} = \frac{D_{Mg} D_{Fe}}{X_{Mg} D_{Mg} + X_{Fe} D_{Fe}} \quad (3)$$

(Florence & Spear, 1995; Ganguly *et al.*, 1998). $D_{Fe\text{-}Mg}$ stands for the inter-diffusion rate of Fe and Mg. D_{Mg} and D_{Fe} are the temperature dependent diffusivites of Fe and Mg as calculated with eq. 2, respectively. X_{Mg} and X_{Fe} represent two concentration ratios of Mg and Fe as described elsewhere in the text, respectively. The outermost node point of the modelled garnet is always in equibrium with the adjacent biotite at $T_{(t)}$ and controlled by the Kd. The Kd is calculated using the thermometer equation of Ferry & Spear (1978):

$$Kd = exp\left(\frac{-\Delta H + T \Delta S}{3 Rt}\right) \quad (4)$$

where enthalpy change $\Delta H = 52107.536$ J and entropy change $\Delta S = 19.506$ JK^{-1}. We note that the original formulation also includes a P-dependent term, which is neglected here. Since the modelled garnets are nearly pure almandine-pyrope solid solutions, the activity model of Ferry & Spear (1978) describes sufficiently the non-ideal behaviour of mixing. X_{Mg}^{Grt} of the outermost node point of the modelled garnet is calculated from Eq. 4 and the Kd expression between garnet and biotite:

$$Kd = \frac{X_{Mg}^{Grt} X_{Fe}^{Bt}}{X_{Fe}^{Grt} X_{Mg}^{Bt}} \quad (5).$$

The diffusion of elements inside the garnet was modelled by numerically solving the spherical form of the one-dimensional diffusion equation:

$$\frac{\partial C}{\partial r} = ln\left(D\frac{\partial^2 C}{\partial r^2} + \frac{2}{r}\frac{\partial C}{\partial r}\right) \quad (6)$$

using a Crank-Nicolson finite difference approach. Diffusion of Fe and Mg in biotite is assumed to be several oders of magnitude faster than in garnet, so that chemical zonation in biotite can be neglected. The accuracy of our approach was tested using Dodson's equation (Dodson, 1986):

$$\frac{Q}{RT_c} = ln(\alpha \frac{D_0}{r^2} \frac{RT_c^2}{Qs}) \quad (7)$$

in which T_c is the closure temperature, r is the grain radius, and α is an adjustable parameter which is $\alpha = 7.1$ for closure at the grain center and for spherical geometry (Dodson, 1986).

In order to accommodate the fact that the volumetric ratio of biotite to garnet is not large, the mass balance needs to be considered. Mass balance is described by:

$$n_{tot}^{Fe} = m_{Grt} n_{Grt}^{Fe} + m_{Bt} n_{Bt}^{Fe} \quad (8),$$

$$n_{tot}^{Mg} = m_{Grt} n_{Grt}^{Mg} + m_{Bt} n_{Bt}^{Mg} \quad (9),$$

$$n_{Grt}^{Fe} + n_{Grt}^{Mg} = constant \quad (10),$$

$$n_{Bt}^{Fe} + n_{Bt}^{Mg} = constant \quad (11),$$

where: n_{tot}^{i} is the total number of moles in species i; i = Fe, Mg, m_j is the number of moles of phase j; j = garnet and biotite and n_j^i is the number of moles of species i in phase j. Using these equations and the Kd expression in Eq. 5, Fe and Mg values at the metamorphic peak were retrieved for garnet and biotite (Table 3). In the numerical calculations, mass balance between garnet and biotite is achieved by calculating the flux of Fe and Mg at each time step and setting a new X_{Mg} for biotite. Numerical calculations for finite grain size were tested against the modification of Dodson's equation by Ehlers & Powell (1994):

$$\frac{Q}{RT_c} = ln(\alpha \frac{D_0}{r^2} \frac{RT_c^2}{Qs}) + \beta\, ln(1 + \frac{1}{zKd}) \quad (12),$$

where $z = \frac{r_{Bt}}{r_{Grt}}$ and α was set to 2.56 and β to 1.72.

Note, that both, our numerical model and the analytical solution of Ehlers & Powell (1994) implicitly assume that (a) the garnet crystal is totally surround by biotite or the diffusion along grain boundaries is faster than diffusion within garnet; (b) no growth or resorption occurred during cooling. The numerical model treats the garnet crystal as nearly spherical while the analytical solution uses a plane sheet model.

References

Appel, P., Möller, A., Schenk, V. (1998): High-pressure granulite facies metamorphism in the Pan-African Belt of eastern Tanzania; P-T-t evidence against granulite formation by continent collision. *J. metamorphic Geol.*, **16**, 491-509.

Bauernhofer, A.H. (2003): Tectonic ambience of early to late Pan-African structures from the Mozambique belt in SE-Kenya and NE-Tanzania. *Doctoral thesis*, University Graz, pp. 135.

Bhattacharya, S. & Kar, R. (1998): Structural constraints on reworking in the Western Ghats granulite belt, India, and the Antarctic analogue. *Gondwana Research*, **1**, 285-290.

Berman, R.G. & Brown, T.H., (1992): Thermobarometry with estimation of equilibration state [TWEEQU]: a software package for IBM or compatible personal computers. *Geological Survey of Canada*, Report, p. 2534.

Cygan, R.T. & Lasaga, A.C. (1985): Self-diffusion of magnesium in garnet at 750-900°C. *Am. J. Sci.*, **285**, 328-350.

Dachs, E. & Proyer, A. (2002): Constraints on the duration of high-pressure metamorphism in the Tauern Window from diffusion modelling of discontinuous growth zones in eclogite garnet. *J. Metamorphic Geol.*, **20**, 769-780.

Dodson, M.H. (1973): Closure temperature in cooling geochronological and petrological systems. *Contrib Mineral. Petrol.*, **40**, 259-274.

— (1986): Closure profiles in cooling systems. *Materials Science Forum*, **7**, 145-154.

Ehlers, K. & Powell, R. (1994): An empirical modification of Dodson's equation for closure temperature in binary systems. *Geochim. Cosmochim. Acta*, **58**, 241-248.

Eiler, J.M., Baumgartner, L.P., Valley, J.W. (1992): Intercrystalline stable isotope diffusion: a fast grain boundary model. *Contrib. Mineral. Petrol.*, **112**, 534-557.

Eiler, J.M., Valley, J.W., Graham, C.M., Baumgartner, L.P. (1995): The oxygen isotope anatomy of a slowly cooled metamorphic rock. *Am. Mineral.*, **80**, 757-764.

Fernando, G.W.A.R., Hauzenberger, C.A., Baumgartner, L.P., Hofmeister, W. (2003): Retrograde diffusion zoning in garnet: Implications for three-stage cooling history of mafic granulites in Highland Complex of Sri Lanka. *Min. Petrol.*, **78**, 53-71.

Ferry, J.M. & Spear, F.S. (1978): Experimental calibration of the partitioning of Fe and Mg between biotite and garnet. *Contrib. Mineral. Petrol.*, **66**, 113-117.

Florence, F.P. & Spear, F.S. (1995): Intergranuler diffusion kinetics of Fe and Mg during retrograde metamorphism of a pelitic gneiss from the Adirondack mountains. *Earth Planet. Sci. Lett.*, **134**, 329-340.

Ganguly, J., Cheng, W., Chakraborti, S. (1998): Cation diffusion in aluminosilicate garnets: experimental determination in pyrope-almandine diffusion couples. *Contrib. Mineral. Petrol.*, **131**, 171-180.

Ganguly, J., Dasgupta, S., Cheng, W., Neogi, S. (2000): Exhumation history of a section of the Sikkim Himalayas, India: records in the metamorphic mineral equilibria and compositional zoning. *Earth Planet. Sci. Lett.*, **183**, 471-486.

Ganguly, J., Hensen, B.J., Cheng, W. (2001): Reaction texture and Fe-Mg zoning in granulite garnet from Sostrene Island, Antarctica; modeling and constraint on the time scale of metamorphism during the Pan-African collisional event. *Proc. Indian Academy of Sciences*: *Earth Planet. Sci.*, **110**, 305-312.

Hauzenberger, C.A. (2003): Mineralogy, petrology and geochronology of the Mozambique belt of SE-Kenya and SW-Tanzania, East Africa. *Habilitationsschrift*, University Graz, 180 pp.

Holmes, A. (1951): The sequence of pre-Cambrian orogenic belts in south and central Africa. *In*: Sandford, K.S. and Blondel, F. (eds.), 18th *International Geological Congress*, London, **Part XXIV**, 254-269.

Horkel, A., Niedermayr, G., Wachira, J.K., Pohl, W., Okelo, R.E., Nauta, W.J. (1979): Geology of the Taita Hills, Coast Province/Kenya. *Geol. Survey Kenya,* Nairobi, **102**, pp. 33.

Jacobs, J., Fanning, C.M., Henjes-Kunst, F., Olesch, M., Paech, H.-J. (1998): Continuation of the Mozambique belt into East Antarctica: Grenville age metamorphism and polyphase Pan-African high grade events in central Dronning Maud Land. *J. Geol.*, **106**, 385-406.

Kretz, R. (1983): Symbols for rock forming minerals. *Am. Mineral*., **68**, 277-279.

Lasaga, A.C. (1983): Geospeedometry: An extension of geothermometry. *In*: Saxena S.K. (ed) «Kinetics and equilibrium in mineral reactions». *Adv. Phys. Geochem.*, **3**, 243-284.

Lee, J.K. (1993): The argon release mechanisms of hornblende in vacuo. *Chemical Geol.*, **106**, 133-170.

Maboko, M.A.H. & Nakamura, E. (1995): Sm-Nd garnet ages from the Uluguru granulite complex of eastern Tanzania: further evidence for post-metamorphic slow cooling in the Mozambique belt. *Precamb. Res*., **74**, 195-202.

Markl, G., Baeuerle, J., Grujic, D. (2000): Metamorphic evolution of Pan-African granulite facies metapelites from southern Madagascar. *Precamb. Res*., **102**, 47-68.

Mezger, K., Essene, E.J., Halliday, A.N. (1992): Closure temperature of the Sm-Nd system in metamorphic garnets *Earth Planet. Sci. Lett*., **113**, 397-409.

Möller, A., Mezger, K., Schenk, V., (2000): U-Pb dating of metamorphic minerals: Pan-African metamorphism and prolonged slow cooling of high pressure granulites in Tanzania, East Africa. *Precamb. Res*., **104**, 123-146.

O'Brian, P. (1997): Garnet zoning and reaction textures in overprinted eclogites, Bohemian Massif, European Variscides: A record of their thermal history during exhumation. *Lithos*, **41**, 119-133.

Parkinson, J. (1947): Outline of the Geology of the Mtito-Tsavo Area, Kenya. *Geol. Survey Kenya*, Nairobi, **13**, pp. 40.

Pohl, W. & Niedermayr, G. (1979): Geology of the Mwatate Quadrangle and the Vanadium Grossularite Deposits of the area. *Geol. Survey Kenya*, Nairobi, **101**, pp. 55.

Powell, R. & White, L. (1995): Diffusive equilibration between minerals during cooling; an analytical extension to Dodson's Equation for closure in one dimension. *Geol. J.*, **30**, 297-305.

Raase, P. & Schenk, V. (1994): Petrology of granulite-facies metapelites of the Highland Complex, Sri Lanka; implications for the metamorphic zonation and the P-T path. *Precamb. Res.*, **66**, 265-294.

Shackleton, R.M., (1996): The final collision zone between East and West Gondwana: where is it? *J. Afr. Earth Sci*., **23**, 271-287.

Sommer, H., Kröner, A., Hauzenberger, C.A., Muhongo, S., (2003): Metamorphic petrology and zircon geochronology of high-grade rocks from thecentral Mozambique belt of Tanzania. *J. metamorphic Geol.*, **21**, 915-934.

Stern, R.J. (1994): Arc assembly and continental collision in the Neoproterozoic East African Orogen: implications for the consolidation of Gondwanaland. *Annual Reviews Earth Planet. Sci.*, **22**, 319-354.

Stüwe, K. & Sandiford, M. (1993): A preliminary model for the 500 Ma event in the East Antarctic Shield. *Intern. Gondwana Symposium*, **8**, 125-130.

Received 23 September 2003
Modified version received 1 October 2004
Accepted 27 October 2004